Slalom-tailoring haptic piloting assistance: A comparison between an static force field-based design and a design inherited from human motion

Yale Lee
yale.lee@onera.fr
PhD candidate
ONERA
Salon-de-Provence, France

Thomas Rakotomamonjy
thomas.rakotomamonjy@onera.fr
Senior Research Scientist
ONERA
Salon-de-Provence, France

Abstract

Haptic flight controls have been extensively studied across various applications over the last years. This study focuses on the slalom task as defined by ADS-33F, an obstacle avoidance scenario. We examine two haptic designs derived from a common model of obstacle repulsion and goal attraction. The first design is based on a force field, representing an information processing approach that adjusts force feedback according to the distance to obstacles. The second design follows an ecological approach, inspired by goal-steering dynamics in human walking. Both designs were tested using a Pilot-in-the-Loop simulator with various gate configurations to modulate geometrical difficulty, and two control modes to examine the impact of the Controlled Element's dynamics. The results are analyzed in terms of average Cycle Time, velocity, acceleration, and applied force. Sidestick activity is modeled using Mottet's model of human arm kinematics . Participants also completed a NASA-Task Load Index questionnaire after each trial to evaluate perceived task load. This paper presents initial findings from a study involving 10 participants.

ABBREVIATIONS AND NOTATIONS

AP	Auto-Pilot
FBW	Fly-by-Wire
FCC	Flight Control Computer
FE	Flight Envelope
FEP	Flight Envelope Protection
FPG	Flight Path Guidance
HOTAS	Hands-On-Throttle-And-Stick
HUD	Head-Up Display
NASA-TLX	NASA Task Load indeX
PAV	Personal Air Vehicle
PitL	Pilot-in-the-Loop
UAM	Urban Air Mobility
VR	Virtual Reality
VRS	Vortex Ring State
CE	Controlled Element
SA	Situational Awareness

Table 1: Abbreviations

W	Slalom gate width, m
H	Lateral gate distance, m
L	Longitudinal gate distance, m
CT	Cycle Time, s
ID	Index of Difficulty, $bits$
MT	Movement Time, s

Table 2: Notations from Fitts's paradigm [1]

ϕ	Apparent velocity heading, rad
b	Damping on velocity heading, s
x	Aircraft position along x-axis, m
y	Aircraft position along y-axis, m
ψ_G	Apparent goal heading, rad
k_G	Goal stiffness, s^2
c_1	Goal distance exponential decrease rate, m^{-1}
c_2	Minimum acceleration factor
d_G	Distance to goal, m
ψ_O	Apparent obstacle heading, rad
k_O	Obstacle stiffness, s^2
c_3	Obstacle heading exponential decrease rate, rad^{-1}
c_4	Obstacle distance exponential decrease rate, m^{-1}
d_O	Distance to obstacle, m

Table 3: Notations from behavioural dynamics model of human walking [3]

c_{10}	Linear stiffness coefficient, s^{-2}
c_{30}	Duffing cubic stiffness coefficient, $m^{-2} \cdot s^{-2}$
c_{01}	Linear damping coefficient, s^{-1}
c_{03}	Rayleigh cubic damping coefficient, $s \cdot m^{-2}$

Table 4: Notations from human arm kinematics model [2]

1 INTRODUCTION

As for its unstable nature, piloting a rotorcraft is a sophisticated task, requiring critical capacities of synthesis and a sharp sense of Situational Awareness (SA). In the additional context of Urban Air Mobility (UAM), piloting assistance is a compulsory prerequisite both for security and efficiency purposes with Personal Air Vehicles (PAV) specifically aiming for novice operators. In line with Hegg et al. [4], active inceptors are investigated to enhance piloting experience. Indeed, many works investigate how flight controls can benefit from haptic sidesticks. Focusing on manned flight, they can be classified under 3 main categories:

1. Augmented perception providing enhanced measurements derived from Flight Control Computers (FCC) sensors
2. Flight Envelope Protection (FEP) based on aggregated quantities
3. Flight Path Guidance (FPG) with prediction of future state

On a task of slalom more specifically, augmented perception of FPG seem particularly appropriate strategies. Yet, to our knowledge, very few studies if not compare two designs driven by the same model of goals and obstacles but motivated by different approaches of human perception. Here, we aim to compare the effects of a slalom catering assistance driven either by a computational or an ecological design.

1. A first design directly fed by an electrostatic-inspired force field filling in for the lack of human direct perception of distance (See Figure 1a),
2. A second design following Fajen's behavioural dynamics model of goal-steering in human walking [3], rooted in ecological framework and embodying the belief that human being naturally perceives the capacity to avoid an obstacle and adapts their locomotion (See Figure 2).

2 RELATED WORKS

The dawn of Fly-by-Wire (FBW) by the early 2000s marked the end of mechanical linkage. If this came with a bunch of advantages such as alleviated maintenance, it disrupted the kinesthetic feedback pilots used to have in their sidestick. With the recent maturation of active inceptors, following the path of robotic teleoperation to benefit from haptic sidesticks to fill for the lack of kinesthetic feedback seems a promising approach. Several studies have submitted various design and approaches. This section suggests a three-fold classification based on the type of information returned through the haptic sidestick.

2.1 Augmented perception

The first type of information that comes to mind is a piece that augments human limited perception range [5], [6]. More precisely, restored quantity can be an angle of attack, particularly tricky for a pilot to estimate yet paramount for the control of a fixed-wing aircraft [7], a bank angle [8], the pitch [8] and the roll [9]. Another possibility is to pass the status of the internal elements such as engine [10], [11], or the information of distance for the avoidance of obstacles [12], [13], [14], [15], [16], [17], [18] ,[19], [20], [21], [22], [23] by benefiting from extended localization and distance estimation capacities required in FCC. It is very well represented in existing studies as the gain is quite clear-cut.

2.2 Aggregated quantities

Piloting is well-known for being a task difficult to perform, particularly due to the amount of values to monitor and process for a fine piloting experience. Not only is human being limited in their perception range, but they also lack computing and calculating capacities when it comes to aggregating various quantities and determine the limits of aircraft controllability. Thus this second type which encompasses FEP functionalities. Determining the limits of Flight Envelope (FE) requires synthesizing criteria on many cross-dependant variables such as angle of attack, velocity, load factors, making the decision particularly trickly to understand even when the Auto-Pilot (AP) or some form of assistance takes to call. On fixed-wing designs, Van Baelen exploited active sidesticks to indicate FE vicinity but also break down the cause behind such result from FCC [24], [25], whereas Horn focused on rotorcraft [26], [27], [28]. Rotorcraft also have the singularity to demonstrate a very dangerous state called Vortex Ring State (VRS) where the aircraft stalls in its own cell of air despite maintaining local lift. This occurs when the vertical descent speed is high and pilots struggle to identify it whereas it calls for immediate correction. So active sidesticks are also investigated to help awareness in such conditions [29], [30], [31].

2.3 Prediction of future state

Eventually, all this awareness calls for some corrective action. This is the third type: a prediction of future state and how modifying it can correct current situation. Designs are precisely tailored to each flight control system so they vary in resolution methods, application range and operation conditions. Yet, most follow one of these goals:

- enforce a new trajectory! [32], [33], [34], [35],
- integrate current state in the prediction by inverting the model of flight dynamics: [31], [27], [28], [10], [36]
- implement the concept of FPG by providing prediction on larger time scale: [37], [26], [38].

Though, despite the wide range of designs, current works struggle to achieve acceptability.

3 HAPTIC ASSISTANCE DESIGNS

Here, we focus on a task of slalom derived from ADS-33F [39] and propose a design based on a goal-steering model of human walking to compare against an existing force field based design.

3.1 Electrostatic-inspired force field design $H1$

This design is quite common to achieve obstacle avoidance even though the definition of the obstacle may differ: the obstacle may be physical [16], [20], [21], [22], [23], or represent a virtual area to avoid. Obstacles are modelled as repulsive areas with positive potential so the potential is high at their location. Therefore, the derived force pushes the system away from these specific locations. Additionally, objective to pursue can be modelled as an attractive hence negative potential so the derived force will apply supplementary guidance.

$$f(x;y) = -\frac{k_G}{\sqrt{d_G^2 + k_G^2}} + \frac{k_O}{\sqrt{d_O^2 + k_O^2}}$$
$$\vec{F}(x;y) = -\overrightarrow{\nabla f}(x;y) = \left(-\frac{\partial f}{\partial x}; -\frac{\partial f}{\partial y}\right)$$

where

- f the candidate potential function with a negative term for goal attraction and a positive term for obstacle repulsion (See Figure 1b),
- $\vec{F} = -\overrightarrow{\nabla f}$ the corresponding force field (See Figure 1c

with

- $(d_G; d_O)$ the aircraft distances to goal and obstacles respectively
- $(k_G; k_O)$ the goal attraction and obstacle repulsion stiffness coefficients

Computed x- and y-axis components F_x and F_y of the force field (See Figure 1c) are directly fed to the actuation of the sidestick so it pushes the operator away from obstacles and towards the middle of the gate to come in real time. In other words, at a given position $(x; y)$, the sum of every gate repulsive force and the attractive force of the upcoming gate is applied. Therefore, this design could be classified as an aggregated quantity.

3.2 Goal-steering dynamics design $H2$

In [3], Fajen utilizes so-called behavioural dynamics model to characterize human walking route selection when goal-steering while avoiding obstacles.

More specifically, path is proved to follow a second-order dynamics on velocity heading (1), given constant

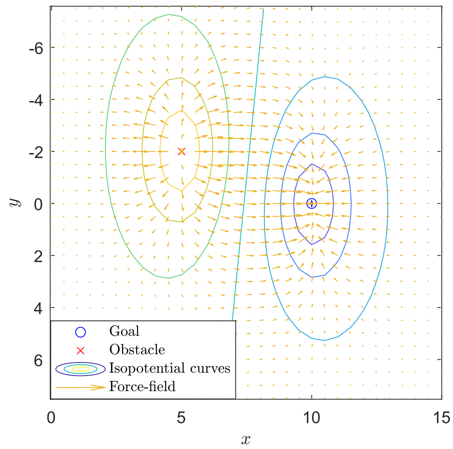

(a) Electrostatic-inspired isopotential curves and force field

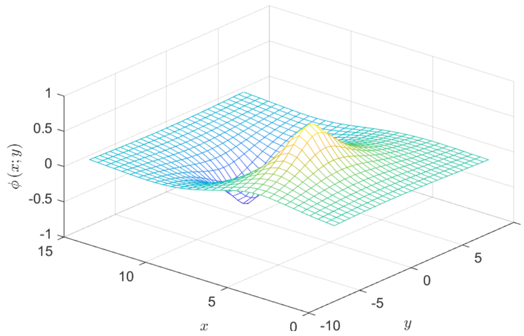

(b) Electrostatic-inspired potential function f

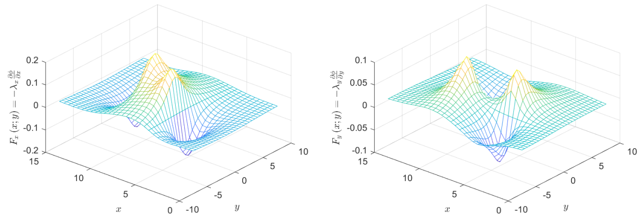

(c) x- and y-axis components F_x and F_y of electrostatic-inspired force field F (derived from potential function f)

Fig. 1: Electrostatic-inspired force field design

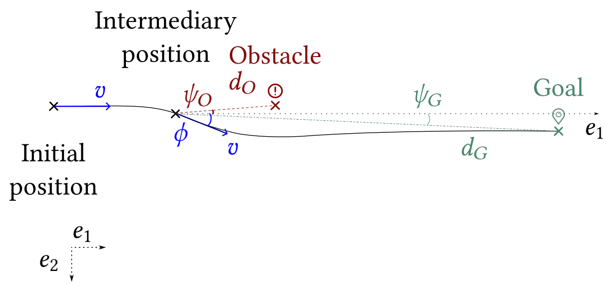

Fig. 2: Goal-steering dynamics design

speed $\|\vec{v}\|$. The direction of initial velocity vector defines an exocentric frame of reference, and every distance and heading direction is defined w.r.t. this frame.

$$\begin{pmatrix} \dot{\phi} \\ \ddot{\phi} \\ \\ \dot{x} \\ \dot{y} \end{pmatrix} = \begin{pmatrix} \dot{\phi} \\ -b\dot{\phi} - k_G\left(\phi - \psi_G\right)\left(e^{-c_1 d_G} + c_2\right) \\ +k_O\left(\phi - \psi_O\right) e^{-c_3\left|\phi - \psi_O\right|} e^{-c_4 d_O} \\ cos(\phi)\sqrt{\dot{x}^2 + \dot{y}^2} \\ sin(\phi)\sqrt{\dot{x}^2 + \dot{y}^2} \end{pmatrix} \quad (1)$$

with

- $(\vec{e}_1; \vec{e}_2)$ the orthonormal system of coordinates defined by the initial vector of velocity
- ϕ the aircraft velocity heading expressed in inertial frame (See Figure 2)
- $(\psi_G; \psi_O)$ the aircraft heading to goal and obstacles respectively (See Figure 2)
- $(d_G; d_O)$ the distance to goal and obstacles respectively (See Figure 2)
- b the steering damping coefficient embodying human motion inertia
- $(k_G; c_1; c_2)$ the goal attraction stiffness embodying convergence rate, exponential decay rate to goal distance and minimum velocity heading acceleration
- $(k_O; c_3; c_4)$ the obstacle repulsion stiffness embodying divergence rate, exponential decay rate to obstacle distance and exponential decay rate to obstacle heading

This model is used to define the second haptic design $H2$. Every $500ms$, the behavioural dynamics model is fed with current state of the virtual environment (x- and y-axis components of translational velocity $\dot{x}$ and $\dot{y}$, current position), computes corresponding velocity heading ϕ (2), goal and obstacle heading ψ_G (3) and ψ_O (4), and distances d_G (5)and d_O (6).

$$\phi = \tan^{-1}\left(\frac{\dot{y}}{\dot{x}}\right) \quad (2)$$

$$\psi_G = \tan^{-1}\left(\frac{y_G - y}{x_G - x}\right) \quad (3)$$

$$\psi_O = \tan^{-1}\left(\frac{y_O - y}{x_O - x}\right) \quad (4)$$

$$d_G = \sqrt{\left(x_G - x\right)^2 + \left(y_G - y\right)^2} \quad (5)$$

$$d_O = \sqrt{\left(x_O - x\right)^2 + \left(y_O - y\right)^2} \quad (6)$$

$$\quad (7)$$

Updated model is resolved using a Runge-Kutta first order solver over $2500ms$ so the expected dynamics is predicted. At each time step within this range, predicted position or velocity is fetched based on control mode and directly fed to the active sidestick so the participant is guided to follow this expected dynamics.

This design, in opposition with the electrostatic-inspired force field design helps the operator identify the expected direction to come and thus should be classified under prediction of future state.

4 EXPERIMENTAL DESIGN

4.1 Task

This is a task of slalom conducted in Virtual Reality (VR) for which the operator is represented in the cockpit, piloting an aircraft using the sidestick (See Figure 5a). The goal is to pass every gate, as fast as possible. All gates are represented by light poles in an urban-tinted environment (See Figure 5b). If every gate is passed, the participant is asked to answer a NASA-TLX questionnaire using the throttle lever (See Figure 5a).

4.2 Participants

To this day, the results of 10 participants are gathered.

	Force field design $H1$	Goal-steering design $H2$
Age	$\mu = 27.00$ $\sigma = 5.02$	$\mu = 24.88$ $\sigma = 4.48$
Gender	$F = 2$ $M = 5$	$F = 1$ $M = 7$
Handedness	$L = 2$ $R = 5$	$L = 0$ $R = 8$
Experience in PC gaming	None = 2 Low = 2 Medium = 1 High = 2	None = 1 Low = 1 Medium = 1 High = 5

Table 5: Participant profiles

4.3 Slalom configurations

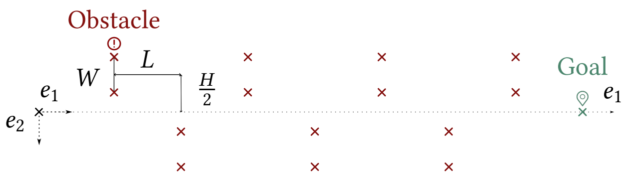

Fig. 3: Definition of geometrical quantities defining task of slalom

Different combinations of gate width W, longitudinal distance L and lateral distance to center $\pm\frac{H}{2}$ (See Figure 3) are considered to extend the scope of slalom definition from ADS-33 by utilizing Fitts' Index of Difficulty (ID) [1] as an objective measurement of the inner difficulty of the slalom task (See Equation 9). Supposing a fixed gate width $W = 5m$, 5 different combinations of $(H; L)$ are tested, which brings varying gate-to-gate distance $D = \sqrt{H^2 + L^2}$ (See Table 6).

Latest works on this paradigm suggest an expression of ID covering dependency to H and W only (See Equation 8).

$$ID = \log_2\left(1 + \frac{H}{W}\right) \quad (8)$$

However, in our protocol, the impact of modulating L along forward axis is necessary so we here use the expression presented in Equation (9) which has been established preliminarily using the same empirical approach as Fitts' original expression: by identifying an expression so ID shares a linear relation with CT.

$$ID = \log_2 \left(1 + \frac{H}{W} + \frac{H}{L}\right) \quad (9)$$

Therefore, scenes A, B, C can be grouped in a lateral group as ID increases as lateral distance H increases, whereas scenes B, E, D are in longitudinal group as ID increases as longitudinal distance L decreases. A subtlety worth underlining here is that D increases along ID in the lateral group, whereas it decreases in the longitudinal group.

		L		
		$2.5m$	$5m$	$7.5m$
H	$20m$	scene A $D = 20.16m$	scene B $D = 20.62m$	scene C $D = 21.36m$
	$15m$		scene E $D = 15.81m$	
	$10m$		scene D $D = 11.18m$	

Table 6: $(H; L)$ combinations

4.4 Control modes

Additionally, two control modes are considered in order to secern the effects of intermediate control laws dynamics:

1. A position control in which sidestick position measurement directly increments the aircraft position
2. A velocity control where sidestick position represents aircraft velocity

Note both controls are equivalent to closed-loop stabilized flight controls as classical open-loop designs are deemed too complex for novice operators as a first approach study, and would corrupt difficulty regulation through the series of geometrical configurations. Upcoming works may consider implementing more direct manual control designs, hence examining the impact of nonlinear dynamics on the overall HQ acceptability.

4.5 Subjective task load assessment

The NASA-TLX questionnaire [40] is also submitted at the end of each slalom to assess perceived task load in order to identify a correlation with the objective criteria presented in Section 5.1. This questionnaire gathers 6 independent dimensions (See Table 7). The most thorough version includes a weighting step where each possible pair of dimensions is compared. However, this is a heavy process to undergo on every trial which may jeopardize participants' involvement to the task so this study performs a RAW-TLX [41] by averaging every dimension homogeneously, on top of investigating the impact on each dimension individually. Besides, as French is the mother tongue for most participants, the certified French version [42] is used in this experiment.

Mental demand	Exigence mentale
Physical demand	Exigence physique
Temporal demand	Exigence temporelle
Performance	Performance
Effort	Effort
Frustration	Niveau de frustration

Table 7: Correspondance between dimensions of original NASA-TLX [40] and certified French version of the NASA-TLX questionnaire [42]

4.6 Experimental protocol

The experiment contains two sessions, one for each control mode. Each of these sessions contains three blocks:

1. A first block of *training*. During this block, an auditory feedback is provided at passing each gate (increasing frequency two-tone sound when the gate is passed, decreasing frequency when it is missed), and gates are quite distant so the participant can analyse the situation and correct their trajectory. The aim is to help the participant understand the instructions, get familiar with the simulator including the VR headset and current control mode, and calibrate their own performance.

2. Two identical blocks of *trial*. The blocks are separated only to prevent exceeding 30min duration for a single block. All 5 combinations of gate disposition (See Table 6) are covered 8 times each and evenly distributed between the two blocks.

It makes up to 2 control modes × 5 gate configurations × 8 repetitions each, that is 80 trials for each participant.
Each trial can be broken down into 3 phases:

1. *Acceleration phase* (See Figure 4a) : This is the first phase starting right after the virtual environment is reset, and ends one the three green gates are passed. A velocity gauge vertically displays a green central and two red peripheral areas, and participants are instructed to reach the green area by the time they cross third green gate. The goal of this phase is to ensure all participants start all trials within a given range of forward velocity.

2. *Slalom phase* (See Figure 4b) : This starts as soon as the third green gate is crossed and ends with the final red gate. Each slalom consists of 10 left-to-right-to-left cycles, encompassing 21 gates, starting with a right-hand gate. The goal in this phase is to validate every gate by passing between the two light poles representing it and within minimum time. If one or more gates are missed, the exact same condition is submitted a second time by the time the final red gate is crossed. If the second trial is also missed, that condition is put back into the pool of conditions to be tested and presented further into the block.

3. *Questionnaire phase* (See Figure 4c) : This phase can be reached only by passing every gate in the previous trial phase, upon passing final red gate. If the condition of 100% performance is validated, then the cockpit is unloaded, and all 6 questions of the NASA-TLX questionnaire appear successively as a Head-Up Display (HUD). Top to bottom, current dimension, corresponding horizontal gauge, questions describing current dimension.

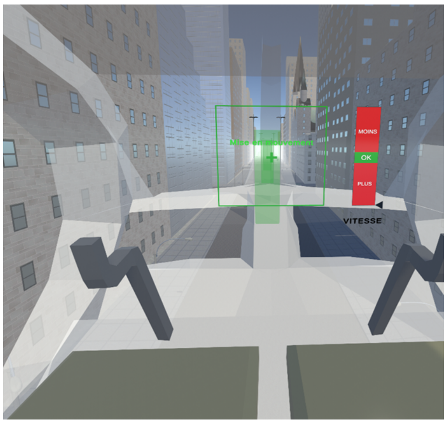

(a) Acceleration phase with velocity gauge on the right hand

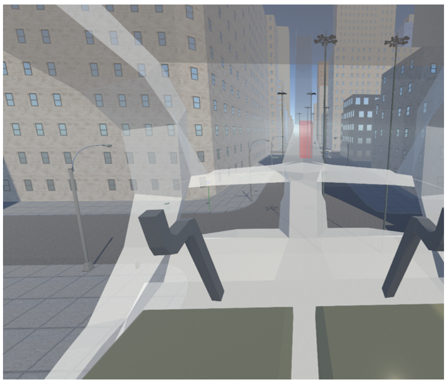

(b) Slalom as seen from operator's point of view

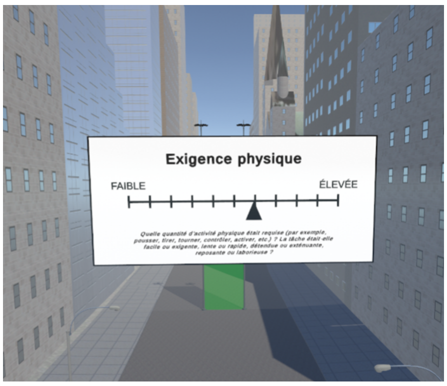

(c) A dimension of the certified French version of NASA-TLX questionnaire

Fig. 4: Visual rendering in virtual scene of simulation

4.7 AIRWISE simulator

This simulator, entirely home-made by ONERA, employs a Thrustmaster WARTHOG™ Hands-On-Throttle-And-Stick (HOTAS) grip actuated by a Brunner CLS-E© motor base, with graphics rendered on a Varjo©VR-3 headset. The software includes a Unity©2020.3 core engine, communicating visuals through the built-in render pipeline via an OpenXR™ standard. The entire simulation operates at a rate of 20*ms*, ensuring that all measurements are sampled at this frequency.

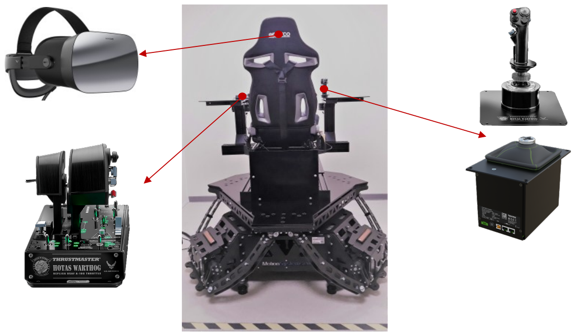

(a) SCHEMERSIVE simulator including VR headset and actuated grip

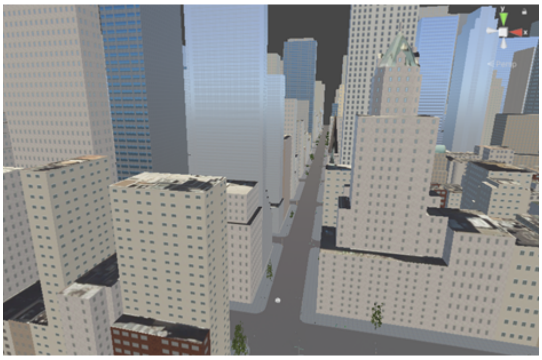

(b) Urban-tinted environment of simulation, as rendered in VR headset

Fig. 5: SCHEMERSIVE, ONERA in-house Pilot-in-the-Loop (PitL) simulator

5 RESULTS & DISCUSSION

Every result figure represents ID along x-axis.

5.1 Objective quantities

5.1.1 *Straight-forward average quantities*

Average Cycle Time (CT)

The easiest quantity to apprehend is CT defined as the time required for the aircraft to pass two consecutive right-hand gates. This quantity derives from the Movement Time MT as in Fitts' paradigm. The result on lateral group (See Figures 6a and 7a) reproduces Fitts' paradigm as CT increases linearly as ID increases. The interesting part is that longitudinal group (See Figure 7b) also shares

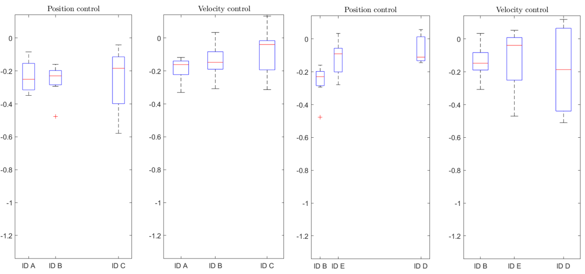

(a) *CT* in lateral group (b) *CT* in longitudinal group

Fig. 6: *CT* in force field $H1$ condition

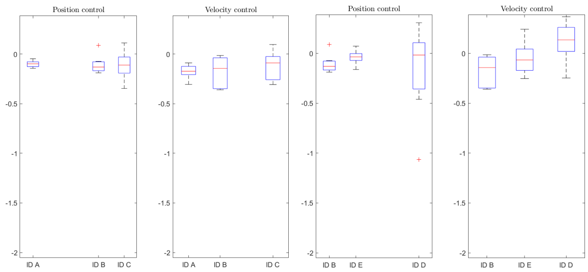

(a) *CT* in lateral group (b) *CT* in longitudinal group

Fig. 7: *CT* in goal-steering dynamics $H2$ condition

that linear relationship. To go further, *CT* is lower in both groups for $H1$ condition (See Figure 6a vs 6b) than $H2$ condition (See Figure 7a vs 7b) which can be interpreted as more intuitive control leaving the door open for faster back and forth cycles. Also, in every group and haptic design, velocity control seems to reach for slightly higher *CT* ranges than position control, all things considered equal. This could be linked to the very dynamics of the control.

Average velocity

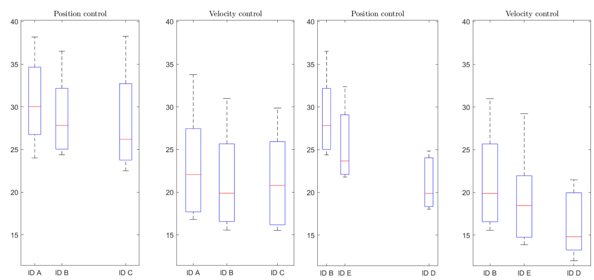

(a) v in lateral group (b) v in longitudinal group

Fig. 8: Average velocity v in force field $H1$ condition

Despite increasing gate-to-gate distance, one would expect average velocity v to decrease along with increasing *CT* given their relation. Results are as expected in lateral group: Figures 8a and 9a show a decrease along *ID* as *CT* increases quite linearly in both position and velocity control, and both $H1$ and $H2$ designs. In longitudinal group though (Figures 8b and 9b), increasing v is expected

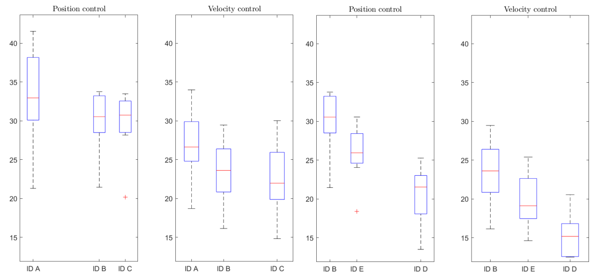

(a) v in lateral group (b) v in longitudinal group

Fig. 9: Average velocity v in goal-steering dynamics $H2$ condition

as *ID* increases due to severely decreasing D (See Table 6). Yet, they decrease in a similar rate than lateral group, suggesting big velocity peaks for lower *ID*. In addition, v is notably lower in velocity control than position control all things considered equal. A possible explanation resides in inner difficulty of velocity control which forces participants to drastically slow down.

Average acceleration

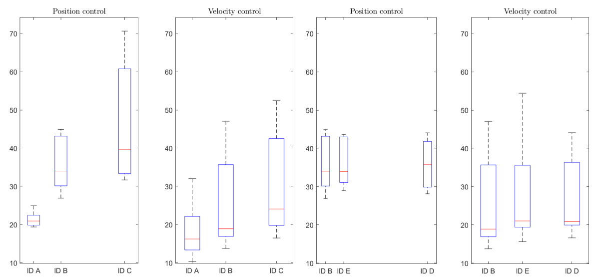

(a) a in lateral group (b) a in longitudinal group

Fig. 10: Average acceleration a in force field $H1$ condition

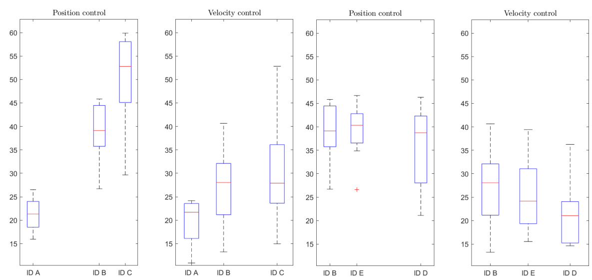

(a) a in lateral group (b) a in longitudinal group

Fig. 11: Average acceleration a in goal-steering dynamics $H2$ condition

Given the relation between velocity and acceleration, the same correlation between average acceleration a and *ID* could be expected. Though, it increases along with *ID* highlighting the occurrence of peaks, probably to gain speed in between gates and partially compensated by braking phases in the vicinity of obstacles (Figures 10a, 11a and 10b), leading to high a in conditions where v can remain low. In Figures 10b and 11b though, position control in longitudinal group on both design, a seems particularly robust to ID as its variation is restrained. As both designs share that characteristics, one can interpret it as an intermediate condition towards velocity control in longitudinal group. Figure 11b displays opposite variation compared to lateral group within similar value range, hinting for higher peaks allowed in low ID whereas difficulty in higher ID enforces low a.

Average applied force

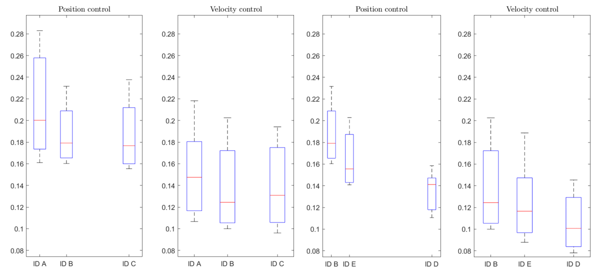

(a) F in lateral group (b) F in longitudinal group

Fig. 12: Average applied force F in force field $H1$ condition

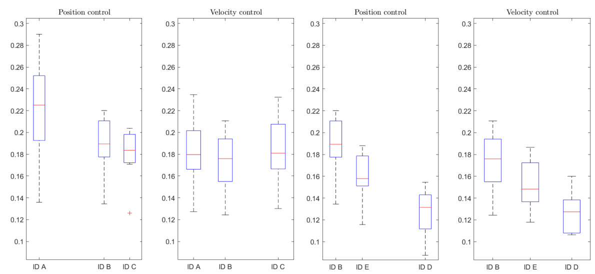

(a) F in lateral group (b) F in longitudinal group

Fig. 13: Average applied force F in goal-steering dynamics $H2$ condition

On initial examination, one can relate high applied force F to tenser piloting experience, with the participant forcing against the assistance. Interestingly, F decreases along ID in all conditions (Figures 12a left-hand, 12b, 13a, 13b) except velocity control in lateral group with design $H2$. This may indicate that participants trust the assistance more and more as the difficulty increases. In such case, the robustness presented in right-hand velocity control in Figure 13a for design $H2$ can be perceived as constant use of the assistance. Now comparing control modes, position control calls for higher values than velocity control so the latter may be harderto control so the participant is relies more on the sidestick. In a similar manner, lateral group scores higher F than longitudinal group but as ID range are not comparable, not much can be inferred. In lateral group, $H1$ brings lower F than $H2$ but results in longitudinal group are the opposite. This could mean lateral group is more compatible to control with design $H1$ whereas design $H2$ is with longitudinal group. One last observation is that F value for low ID in velocity control is similar to the value for high ID in position control with design $H1$. With design $H2$, F range in velocity control within lateral group is very narrow and close to the minimal value of position control; in longitudinal group, F in velocity control is even close to position control. Goal-steering dynamics design $H2$ may have simplified velocity control enough so it becomes close to position control.

5.1.2 *Sidestick activity: Mottet's model of human arm kinematics*

$$\ddot{x} = -c_{10}x + c_{30}x^3 + c_{01}\dot{x} - c_{03}\dot{x}^3 \quad (10)$$

Building on top of Mottet and Bootsma kinematical model of portraits distortion [2], the set of coefficients from Equation (10) is considered a quantitative and objective measurement of control deterioration along ID: the lower the set of coefficients, the more natural hence intuitive the motion involved. For larger values, it either represents a desymmetrization of the left-to-right and right-to-left movements, or the discretization towards a well-defined acceleration phase to reach performance, opposed to a deceleration segment in the vicinity of the goal/obstacle to achieve precision.
Yet, the interpretation is not as straight-forward. The intuitiveness can occur through desymmetrization without discretization, and the over way around. So no conclusion is made regarding the correlation between coefficient value and ID. In addition, only y-axis activity is observed here as the x-axis activity corresponds to back-and-forth displacement and presents no variation in the task of slalom as presented in Section 4.6.

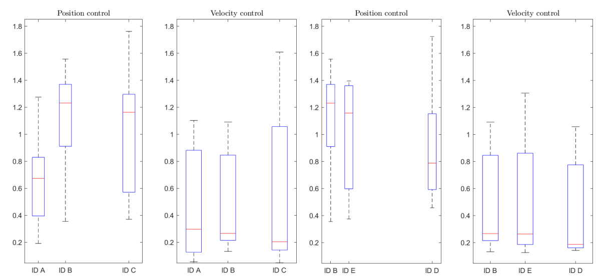

(a) c_{10} along y-axis in lateral group (b) c_{10} along y-axis in longitudinal group

Fig. 14: Linear stiffness c_{10} along y-axis in force field $H1$ condition

Both linear stiffness c_{10} and Duffing cubic stiffness c_{30} present different patterns between design $H1$ and design $H2$. Nevertheless, they have similar evolution within a design (Figures 14, 16, 18 and 20 for $H1$, Figures 15, 17, 19 and 21 for $H2$), meaning piloting degradation expresses in dif-

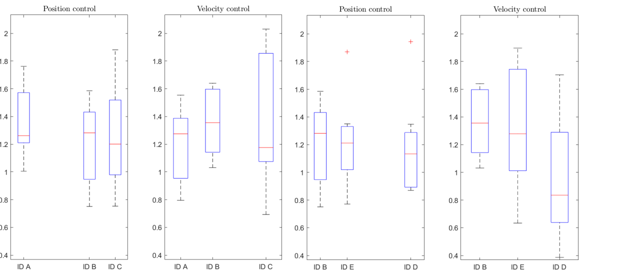

(a) c_{10} along y-axis in lateral group (b) c_{10} along y-axis in longitudinal group

Fig. 15: Linear stiffness c_{10} along y-axis in goal-steering dynamics $H2$ condition

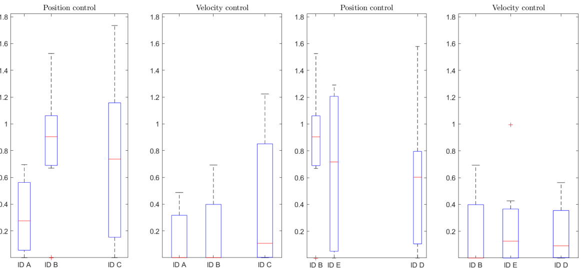

(a) c_{30} along y-axis in lateral group (b) c_{30} along y-axis in longitudinal group

Fig. 16: Duffing cubic stiffness coefficient c_{30} along y-axis in force field $H1$ condition

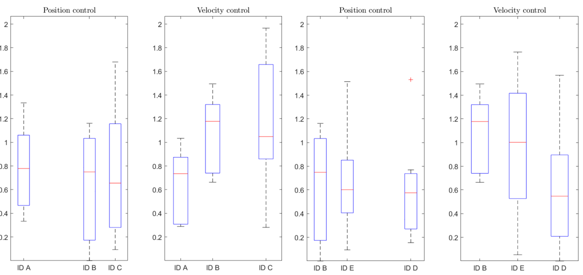

(a) c_{30} along y-axis in lateral group (b) c_{30} along y-axis in longitudinal group

Fig. 17: Duffing cubic stiffness coefficient c_{30} along y-axis in goal-steering dynamics $H2$ condition

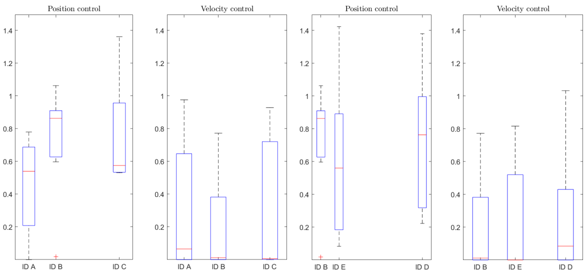

(a) c_{01} along y-axis in lateral group (b) c_{01} along y-axis in longitudinal group

Fig. 18: Linear damping c_{01} along y-axis in force field $H1$ condition

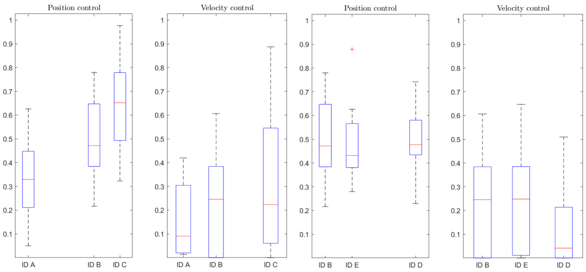

(a) c_{01} along y-axis in lateral group (b) c_{01} along y-axis in longitudinal group

Fig. 19: Linear damping c_{01} along y-axis in goal-steering dynamics $H2$ condition

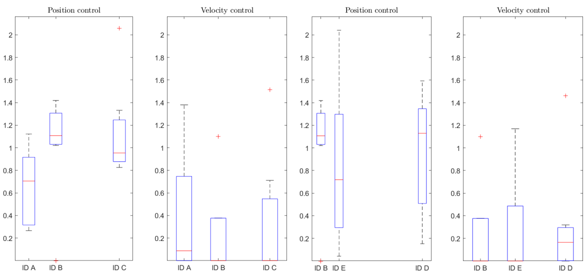

(a) c_{03} along y-axis in lateral group (b) c_{03} along y-axis in longitudinal group

Fig. 20: Rayleigh cubic damping coefficient c_{03} along y-axis in force field $H1$ condition

ferent ways. This is expected as the haptic assistance does have an impact on piloting hence sidestick activity.
With force field $H1$ design, all coefficients show much lower values in velocity control, with a restricted value range. That means, sidestick acceleration is lower in comparison to sidestick velocity and position variations as low coefficients can not build up to large values in Equation 10. In position control, scene B always has the highest coefficient value meaning higher sidestick accelerations, whereas scene E has lowest linear and Rayleigh cubic damping c_{01} and c_{03} respectively. These coefficient embody the distortion of Hooke's portraits so higher value corresponds to more desymmetrized left-to-right and right-to-left activity.
Regarding goal-steering $H2$ design, both stiffness coefficients on the one hand, and both damping coefficients on the other hand have similar correlation to ID, for both control types and groups. Position control in lateral group do not present a clear pattern unlike velocity control which display decreasing linear variations. Both stiffness are higher in velocity control, testifying a more discretized sidestick activity. In the contrary, the correlation is not clear in velocity control on damping coefficients, while the linear correlation to ID is clear in position control. Values are higher in the latter, meaning sidestick activity is more desymmetrized in position control than velocity control.

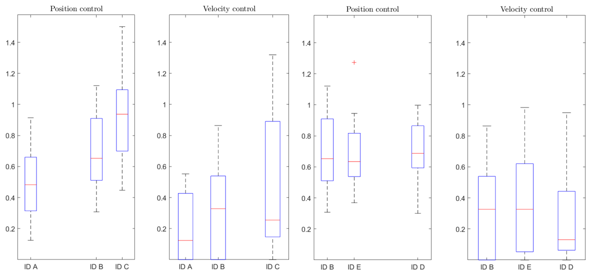

(a) c_{03} along y-axis in lateral group

(b) c_{03} along y-axis in longitudinal group

Fig. 21: Rayleigh cubic damping coefficient c_{03} along y-axis in goal-steering dynamics $H2$ condition

5.2 Subjective quantity

5.2.1 Mental demand

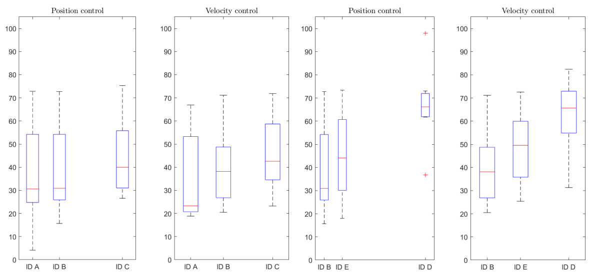

(a) Mental demand in lateral group

(b) Mental demand in longitudinal group

Fig. 22: Mental demand in force field $H1$ condition

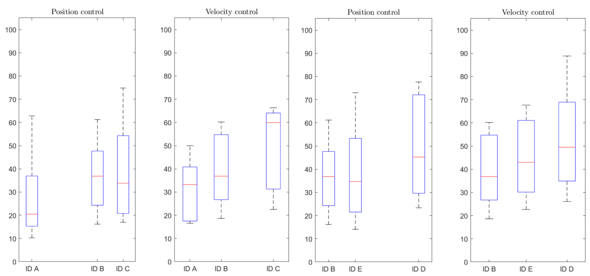

(a) Mental demand in lateral group

(b) Mental demand in longitudinal group

Fig. 23: Mental demand in goal-steering dynamics $H2$ condition

Mental demand increases along with *ID* in every condition, which is expected. Values are higher in velocity control than position control (Figures 22 and 23), with the exception of the lowest *ID* of lateral group with design $H1$ (Figure 22b, left-hand). That specific scene A is indeed very simple to apprehend as many participants voiced it, it could be passed by pushing the sidestick forward and merely tilting it left to right with appropriate frequency. In position control, lateral group values and longitudinal group values are similar with design $H1$ (Figure 22) whereas higher in the longitudinal group with design $H2$ (Figure 23) so the latter may be more demanding in terms of processing and command. Design $H1$ also brings higher mental demand in lateral group, and lower in longitudinal group: the force field $H1$ design may fit the lateral group better as it helps avoid avoidance, whereas goal-steering design $H2$ aims to guide and suits longitudinal group with distantly placed gates better.

5.2.2 Physical demand

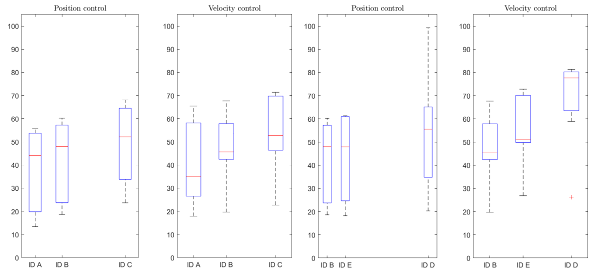

(a) Physical demand in lateral group

(b) Physical demand in longitudinal group

Fig. 24: Physical demand in force field $H1$ condition

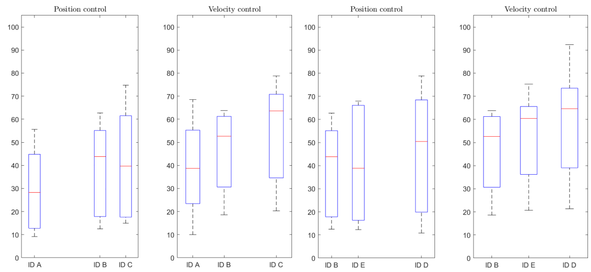

(a) Physical demand in lateral group

(b) Physical demand in longitudinal group

Fig. 25: Physical demand in goal-steering dynamics $H2$ condition

As mental demand, physical demand increases along *ID* except in lateral group in position control with design $H2$ (Figure 25a), meaning increasing difficulty does not only reside in mental load. In lateral group, the value range is lower in position control than velocity control with design $H1$ (Figure 24a) whereas velocity control is higher with design $H2$ (Figure 25a), as if goal-steering assistance on top of velocity control would compensate to equal position control with force field design. Velocity control calls for higher physical demand than position control in the longitudinal group (Figure 25), though design $H2$ reaches lower maximum than design $H1$. Interestingly, physical demand results are in total contradiction with average applied force F, comforting the interpretation from Section 5.1.1 that high values of F represent participant physical involvement, not struggle against the assistance.

5.2.3 *Temporal demand*

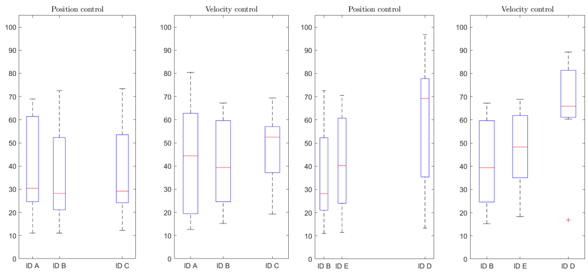

(a) Temporal demand in lateral group

(b) Temporal demand in longitudinal group

Fig. 26: Temporal demand in force field $H1$ condition

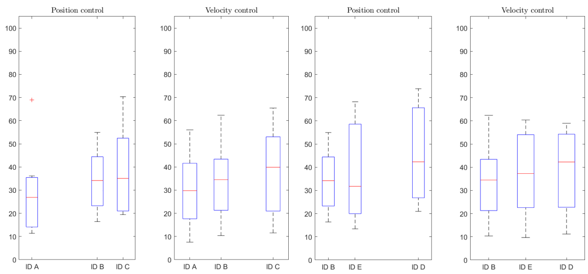

(a) Temporal demand in lateral group

(b) Temporal demand in longitudinal group

Fig. 27: Temporal demand in goal-steering dynamics $H2$ condition

Temporal demand dependency to ID is as expected, that is to say mostly increasing with ID. With design $H1$ (Figure 26), velocity control leads to higher values than position control in both groups, value ranges are quite similar between lateral and longitudinal groups with design $H2$ (Figure 27). Value ranges are also wider with the first design. Goal-steering design $H2$ seems to relieve the pressure on time.

5.2.4 *Performance*

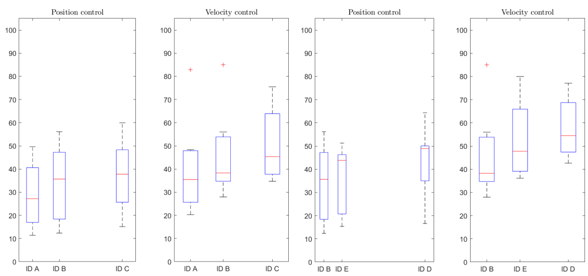

(a) Performance in lateral group

(b) Performance in longitudinal group

Fig. 28: Performance in force field $H1$ condition

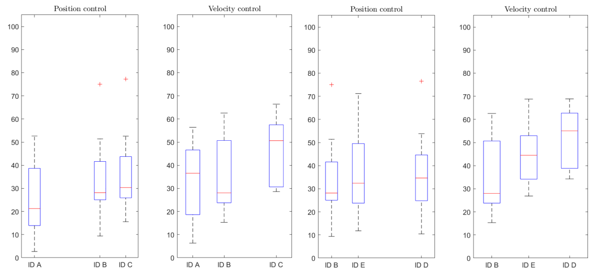

(a) Performance in lateral group

(b) Performance in longitudinal group

Fig. 29: Performance in goal-steering dynamics $H2$ condition

Performance roughly follows ID variation. No clear tendency seems to emerge, possibly due to the presence of outliers. It is worth pinpointing that scene A scores a specially high value in velocity control with design $H2$.

5.2.5 *Effort*

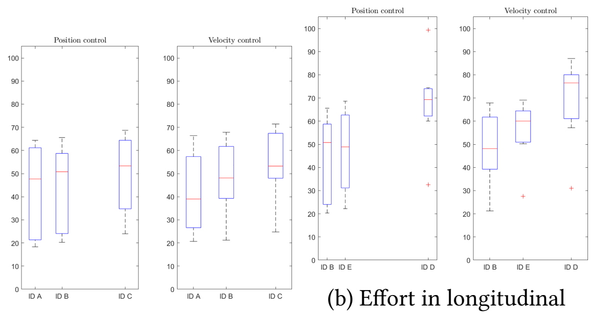

(a) Effort in lateral group

(b) Effort in longitudinal group

Fig. 30: Effort in force field $H1$ condition

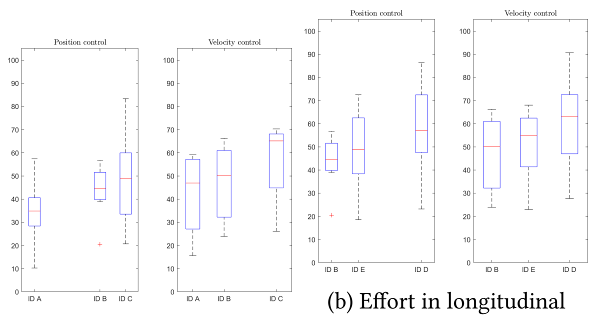

(a) Effort in lateral group

(b) Effort in longitudinal group

Fig. 31: Effort in goal-steering dynamics $H2$ condition

Again, effort is related to ID. Values are higher in longitudinal group. Except the lateral group with design $H1$ (Figure 30a), velocity control requires higher effort, which one can interpret as the force field being directive. All things considered equal, values obtained with design $H1$ (Figure 30) are slightly but consistently higher than design $H2$ (Figure 31)

5.2.6 *Frustration*

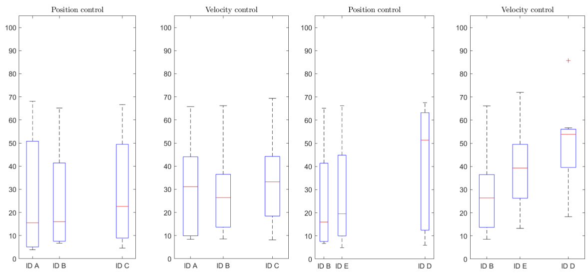

(a) Frustration in lateral group

(b) Frustration in longitudinal group

Fig. 32: Frustration in force field $H1$ condition

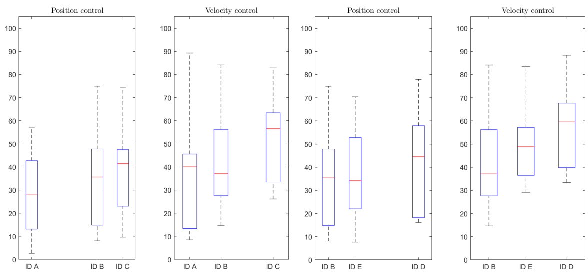

(a) Frustration in lateral group

(b) Frustration in longitudinal group

Fig. 33: Frustration in goal-steering dynamics $H2$ condition

Both groups and both designs show a similar result: position control draws less frustration than velocity control. The difference is lower in lateral group (Figure 32a) than longitudinal group (Figure 32b) with design $H1$, and similar with deisgn $H2$ (Figure 33); again, the goal-steering design brings some homogeneity. Nonetheless, it produces a higher overall frustration level. Notwithstanding human behavioural model, this design appears more difficult for the participants to understand and foresee. A training phase with tighter criteria may overcome this aspect in a next experiment. Besides, scene A in lateral group scores higher frustration than scene B with velocity control, with both $H1$ and $H2$ designs (Figures 32a and 33a, right-hand), despite having lower ID value. This may be the result of cumulated frustration from potentially failing previous trials by pursuing speed over accuracy regardless of the simplicity of the scene.

5.2.7 *RAW-TLX*

Bottom line, RAW-TLX is directly correlated to ID. Design $H1$ is robust to control type with similar value ranges between position and velocity control for both groups (Figure 34). Design $H2$ has slightly higher task load values (Figures 35) but longitudinal group is more robust to ID increase.

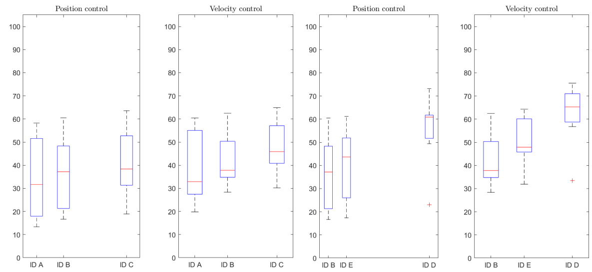

(a) RAW-TLX in lateral group

(b) RAW-TLX in longitudinal group

Fig. 34: RAW-TLX in force field $H1$ condition

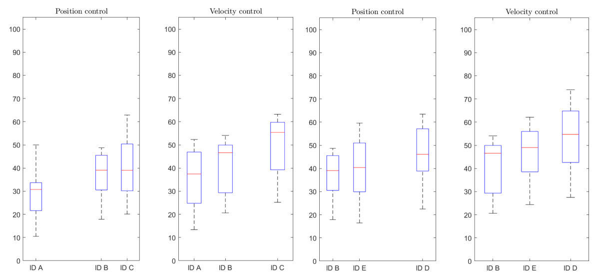

(a) RAW-TLX in lateral group

(b) RAW-TLX in longitudinal group

Fig. 35: RAW-TLX in goal-steering dynamics $H2$ condition

In short, design $H2$ based on goal-steering dynamics seems to be harder to comprehend as it achieves higher mental demand. Yet it maintains similar levels of involvement as force field design $H1$ as measured with physical demand, and provides some relief allowing lower time demand values, for less perceived effort. The level of perceived performance is lower though, which may be related to the higher level of frustration, explaining similar to slightly higher over all task load.

CONCLUSION

We here investigated a new approach to conceive haptic piloting assistance through a design resulting from the resolution of the goal-steering dynamics of human walking. This design is compared against a force field design from existing previous works and conclusion is drawn that it is possible to build an assistance that allows better performance and lower time demand and effort, all while maintaining similar to better levels of involvement. This aspect is paramount as rampant automation pushes operators to more and more passive interactions, leaving the system do the job. The higher levels of mental demand, frustration or even overall task load can thus be interpreted as the price to pay for keeping the operator in the loop.
Moreover, we investigated objective criteria to correlate with subjective questionnaire results in order to identify some criteria for intuitiveness piloting experience. Building on top of Fitts' long-term studied paradigm, we extended the range of potential applications by considering

both lateral and longitudinal groups and the impact on CT, v, a, F on first examination, and even to quantify the sidestick activity. Contradictions in average values emphasize the need for a time-series study of these quantities to identify phases of acceleration and deceleration, how each haptic assistance design impacts the way participants approach each gate. Sidestick activity could also benefit from a distinctive 1^{st} vs 2^{nd} half-cycle study as left-to-right and right-to-left control are asymmetrical.

ACKNOWLEDGMENT

This reasearch is financially supported by the Agence de l'Innovation de Défense (AID 2021.65.0011).

REFERENCES

[1] Paul M. Fitts. "The Information Capacity of the Human Motor System in Controlling the Amplitude of Movement." In: *Journal of Experimental Psychology* 47.6 (1954), pp. 381–391.

[2] Denis Mottet and Reinoud J. Bootsma. "The Dynamics of Goal-Directed Rhythmical Aiming". In: *Biological Cybernetics* 80.4 (Apr. 1999), pp. 235–245.

[3] Brett R. Fajen and William H. Warren. "Behavioral Dynamics of Steering, Obstacle Avoidance, and Route Selection." In: *Journal of Experimental Psychology: Human Perception and Performance* 29.2 (2003), pp. 343–362.

[4] J.W. Hegg et al. "Features of Active Sidestick Controllers". In: *AIAA/IEEE Digital Avionics Systems Conference. 13th DASC.* Phoenix, AZ, USA: IEEE, 1994, pp. 305–308.

[5] Gemma Prieto-Aguilar, Laurent Binet, and Thomas Rakotomamonjy. "DESIGN METHODOLOGY OF FORCE FEEDBACK LAWS THROUGH HELICOPTER CONTROL LOOP SIMULATION". In: (2019), p. 14.

[6] Hassam Ahmed Malik et al. "Effect of Haptic Feedback on Pilot/Operator Performance During Flight Simulation". In: *Applied Sciences* 10.11 (June 2020), p. 3877.

[7] Samantha M. C. Alaimo et al. "Preliminary Evaluation of a Haptic Aiding Concept for Remotely Piloted Vehicles". In: *Haptics: Generating and Perceiving Tangible Sensations.* Ed. by Astrid M. L. Kappers et al. Vol. 6192. Berlin, Heidelberg: Springer Berlin Heidelberg, 2010, pp. 418–425.

[8] J. Ellerbroek et al. "Design and Evaluation of a Flight Envelope Protection Haptic Feedback System". In: *IFAC-PapersOnLine* 49.19 (2016), pp. 171–176.

[9] Samantha M. C. Alaimo et al. "A Comparison of Direct and Indirect Haptic Aiding for Remotely Piloted Vehicles". In: *19th International Symposium in Robot and Human Interactive Communication.* Viareggio, Italy: IEEE, Sept. 2010, pp. 506–512.

[10] Joseph F. Horn and Nilesh Sahani. "Detection and Avoidance of Main Rotor Hub Moment Limits on Rotorcraft". In: *Journal of Aircraft* 41.2 (Mar. 2004), pp. 372–379.

[11] Nilesh A. Sahani et al. "Hub Moment Limit Protection Using Neural Network Prediction". In: *Journal of the American Helicopter Society* 51.4 (2006), p. 331.

[12] T.M. Lam et al. "Effect of Haptic Feedback in a Trajectory Following Task with an Unmanned Aerial Vehicle". In: *2004 IEEE International Conference on Systems, Man and Cybernetics (IEEE Cat. No.04CH37583).* Vol. 3. The Hague, Netherlands: IEEE, 2004, pp. 2500–2506.

[13] T. Mung Lam et al. "UAV Tele-operation Using Haptics with a Degraded Visual Interface". In: *2006 IEEE International Conference on Systems, Man and Cybernetics.* Taipei, Taiwan: IEEE, Oct. 2006, pp. 2440–2445.

[14] T. Mung Lam, Max Mulder, and M. M. (Rene) van Paassen. "Collision Avoidance in UAV Tele-Operation with Time Delay". In: *2007 IEEE International Conference on Systems, Man and Cybernetics.* Montreal, QC, Canada: IEEE, Oct. 2007, pp. 997–1002.

[15] T. Mung Lam, Max Mulder, and Marinus M. van Paassen. "Haptic Interface For UAV Collision Avoidance". In: *The International Journal of Aviation Psychology* 17.2 (Apr. 2007), pp. 167–195.

[16] T.M. Lam et al. "Artificial Force Field for Haptic Feedback in UAV Teleoperation". In: *IEEE Transactions on Systems, Man, and Cybernetics - Part A: Systems and Humans* 39.6 (Nov. 2009), pp. 1316–1330.

[17] T. M. Lam et al. "Force-Stiffness Feedback in Uninhabited Aerial Vehicle Teleoperation with Time Delay". In: *Journal of Guidance, Control, and Dynamics* 32.3 (May 2009), pp. 821–835.

[18] T. Mung Lam, Max Mulder, and Marinus M. van Paassen. "Haptic Interface in UAV Tele-Operation Using Force-Stiffness Feedback". In: *2009 IEEE International Conference on Systems, Man and Cybernetics.* San Antonio, TX: IEEE, Oct. 2009, pp. 835–840.

[19] Samantha Alaimo et al. "Experiments of Direct and Indirect Haptic Aiding for Remotely Piloted Vehicles with a Mixed Wind Gust Rejection/Obstacle Avoidance Task". In: *AIAA Modeling and Simulation Technologies Conference.* Portland, Oregon: American Institute of Aeronautics and Astronautics, Aug. 2011.

[20] Samantha M.C. Alaimo et al. “Evaluation of Direct and Indirect Haptic Aiding in an Obstacle Avoidance Task for Tele-Operated Systems”. In: *IFAC Proceedings Volumes* 44.1 (Jan. 2011), pp. 6472–6477.

[21] Samantha M C Alaimo et al. “Experimental Comparison of Direct and Indirect Haptic Aids in Support of Obstacle Avoidance for Remotely Piloted Vehicles”. In: *Journal of Mechanics Engineering and Automation* (Oct. 2012), p. 10.

[22] Thomas Rakotomamonjy, Laurent Binet, and Mario Müllhäuser. “ONERA-DLR JOINT RESEARCH ON TACTILE CUEING FOR REACTIVE OBSTACLE AVOIDANCE DEDICATED TO LOW SPEED HELICOPTER MANEUVERS”. In: *42nd European Rotorcraft Forum*. Lille, Frankreich, Sept. 2016, p. 14.

[23] L. Binet and T. Rakotomamonjy. “Using Haptic Feedbacks for Obstacle Avoidance in Helicopter Flight”. In: *Progress in Flight Dynamics, Guidance, Navigation, and Control – Volume 10*. Ed. by C. Vallet et al. Krakow, Poland: EDP Sciences, 2018, pp. 47–70.

[24] Dirk Van Baelen et al. “Design of a Haptic Feedback System for Flight Envelope Protection”. In: *Journal of Guidance, Control, and Dynamics* 43.4 (Apr. 2020), pp. 700–714.

[25] Dirk Van Baelen et al. “Flying by Feeling: Communicating Flight Envelope Protection through Haptic Feedback”. In: *International Journal of Human–Computer Interaction* 37.7 (Apr. 2021), pp. 655–665.

[26] Joe Horn, Anthony Calise, and J. Prasad. “Flight Envelope Limiting Systems Using Neural Networks”. In: *23rd Atmospheric Flight Mechanics Conference*. Boston,MA,U.S.A.: American Institute of Aeronautics and Astronautics, Aug. 1998.

[27] Joseph F. Horn, Anthony J. Calise, and J. V. R. Prasad. “Flight Envelope Cueing on a Tilt-Rotor Aircraft Using Neural Network Limit Prediction”. In: *Journal of the American Helicopter Society* 46.1 (Jan. 2001), pp. 23–31.

[28] Joe Horn, Anthony J. Calise, and J. V. R. Prasad. “Flight Envelope Limit Detection and Avoidance for Rotorcraft”. In: *Journal of the American Helicopter Society* 47.4 (2002), p. 253.

[29] Max Abildgaard and L. Binet. “Active Sidesticks Used for VRS Avoidance”. In: 2009.

[30] Laurent Binet et al. “VRS Avoidance as Active Function on Side-Sticks”. In: *American Helicopter Society 65th Annual Forum*. Grapevine, Texas, USA: American Helicopter Society International, Inc., May 2009, p. 19.

[31] Wolfgang Grünhagen et al. “ACTIVE INCEPTORS IN FHS FOR PILOT ASSISTANCE SYSTEMS”. In: (Sept. 2010).

[32] S. de Stigter, M. Mulder, and Marinus M. van Paassen. “Design and Evaluation of a Haptic Flight Director”. In: *Journal of Guidance, Control, and Dynamics* 30.1 (Jan. 2007), pp. 35–46.

[33] Kenneth Goodrich, Ralph Williams, and Paul Schutte. “Piloted Evaluation of the H-Mode, a Variable Autonomy Control System, in Motion-Based Simulation”. In: *AIAA Atmospheric Flight Mechanics Conference and Exhibit*. Honolulu, Hawaii: American Institute of Aeronautics and Astronautics, Aug. 2008.

[34] Kenneth Goodrich, Paul Schutte, and Ralph Williams. “Haptic-Multimodal Flight Control System Update”. In: *11th AIAA Aviation Technology, Integration, and Operations (ATIO) Conference*. Virginia Beach, VA: American Institute of Aeronautics and Astronautics, Septermber 20, 2011.

[35] B. I. Gursky, W. F. J. Olsman, and N. Peinecke. “Development of a Tunnel-in-the-Sky Display for Helicopter Noise Abatement Procedures”. In: *CEAS Aeronautical Journal* 5.2 (June 2014), pp. 199–208.

[36] Mario Müllhäuser and Jeff Lusardi. “US-German Joint In-flight and Simulator Evaluation of Collective Tactile Cueing for Torque Limit Avoidance – Shaker vs. Soft Stop”. In: (2020), p. 18.

[37] Rod Buchanan et al. “Intelligent Flight Path Guidance”. In: June 2005, p. 14.

[38] Frank M. Nieuwenhuizen and Heinrich H. Bülthoff. “Evaluation of Haptic Shared Control and a Highway-in-the-Sky Display for Personal Aerial Vehicles”. In: *AIAA Modeling and Simulation Technologies Conference*. National Harbor, Maryland: American Institute of Aeronautics and Astronautics, Jan. 2014.

[39] Chris L. Blanken et al. *Proposed Revisions to Aeronautical Design Standard - 33E (ADS-33E-PRF) Toward ADS-33F-PRF*. Special Report SR-FCDD-AMV-19-01. Commander, U.S. Army Combat Capabilities Development Command, Sept. 2019.

[40] Sandra G. Hart and Lowell E. Staveland. “Development of NASA-TLX (Task Load Index): Results of Empirical and Theoretical Research”. In: *Advances in Psychology*. Vol. 52. Elsevier, 1988, pp. 139–183.

[41] James C. Byers, Alvah C. Bittner, and Susan G. Hill. “Traditional and Raw Task Load Index (TLX) Correlations: Are Paired Comparisons Necessary?” In: *Advances in Industrial Ergonomical and Safety I*. Vol. 1. Cincinnati, Ohio, U.S.A.: Taylor & Francis, 1989-06-05/1989-06-09, pp. 481–485.

[42] Julien Cegarra and Nicolas Morgado. “Étude des propriétés de la version francophone du NASA-TLX”. In: (Jan. 2009).